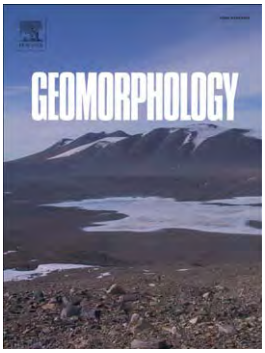

Composite mechanism of the Büyükçekmece (Turkey) landslide as conditioning factor for earthquake-induced mobility

S. Martino, L. Lenti, C. Bourdeau

PII: S0169-555X(16)30840-6
DOI: doi:10.1016/j.geomorph.2018.01.028
Reference: GEOMOR 6310

To appear in: *Geomorphology*

Received date: 7 September 2016
Revised date: 26 January 2018
Accepted date: 27 January 2018

Please cite this article as: Martino, S., Lenti, L., Bourdeau, C., Composite mechanism of the Büyükçekmece (Turkey) landslide as conditioning factor for earthquake-induced mobility, *Geomorphology* (2018), doi:10.1016/j.geomorph.2018.01.028

Composite mechanism of the Büyükçekmece (Turkey) landslide as conditioning factor for earthquake-induced mobility

Martino S.[a*], Lenti L.[b], Bourdeau C.[b]

[a] Dpt. Scienze della Terra and Centro di Ricerca per i Rischi Geologici (CERI), Università di Roma, "Sapienza", P.le Aldo Moro 5, 00185 Roma, Italy
[b] Institut Français des Sciences et Technologies des Transports, de l'Aménagement et des Réseaux (IFSTTAR-Paris) 14-20 Boulevard Newton Cité Descartes Champs sur Marne F-77447 Marne la Vallée Cedex 2, France

[*] Corresponding Author

ABSTRACT

Earthquake-induced displacements of landslides are significantly conditioned by their 1D and 2D interactions with seismic waves, as currently proven by several studies. Nevertheless, the role of a more complex geological setting, responsible for a heterogeneous composition of the landslide mass, can significantly influence these phenomena. The heterogeneity can also depend on multiple phases of the landslide activity, responsible for dislodging the whole landslide mass into submasses, each one delimited by secondary scarps and characterized by individual mobility. Hence, in the framework of the European project "*MARSite – Marmara Supersite: new directions in seismic hazard assessment through focused Earth observation in the Marmara Supersite*", the Büyükçekmece landslide, located approximately 30 km W of Istanbul (Turkey), was considered as a case study. This landslide involves a large mass of approximately 140 million cubic metres, composed of silty clays, tuffs and sands ascribable to Cenozoic geological formations. The landslide is characterized by multiple phases of activity with a composite rototranslational mechanism, which created seven submasses delimited by

secondary scarps. The scheme of water circulation in the landslide slope, based on piezometer data as well as on a geological survey, accounts for two flow nets: the first, shallower flow net is located in superficial sandy deposits, outcropping in the dislodged landslide submasses; the second, deeper flow net is located in the main sliding surface. A slope stability analysis following a global limit equilibrium approach provided a distribution of the pseudostatic coefficient vs. pore water pressure. The results show that the stability of the landslide submasses increases moving downslope, and reactivations are expected in the case of earthquakes with a return period between 475 and 2475 yr, according to the local seismic hazard. Dynamic numerical modelling was also performed using the stress-strain finite difference code FLAC 7.0 to derive the distributions of horizontal displacements vs. characteristic period ratios, defined as the period due to depth (T_s) and total length (T_l) of the landslide mass over the earthquake characteristic period (T_m). The obtained results indicate that an effective characteristic period of the landslide (T_l^*), related to the length of a single counter-slope tilted submass, can provide a more correct explanation for the effect of seismic wave interactions on earthquake-induced displacements. This result indicates that the earthquake-induced mobility of the Büyükçekmece landslide is strongly conditioned by its composite rototranslational mechanisms. In general, these results indicate that landslide evolution can induce a change over time for the characteristic periods related to the dimensions of the dislodged landslide portions and then modify its interactions with seismic waves.

Keywords

Landslide, slope stability, earthquake-induced displacements

1. INTRODUCTION

The behaviour of slopes during earthquake shaking and the induced landslide mobility depend on their complex interactions with seismic waves. Such interactions are controlled by several features including the slope geometry, the landslide mass properties and the physical characteristics of the seismic waves (Bourdeau and Havenith, 2008; Lenti and Martino, 2012; Fotopoulou and Pitilakis, 2015; Martino et al., 2016b). Earthquake reactivated landslides more commonly involve coherent soils or debris. Although these events are a priori recognizable by typical landforms or historical chronicles that document their past activation, much effort is required to evaluate how their stability conditions change due to earthquake occurrences as well as to quantify their coseismic or postseismic mobility in terms of expected displacements.

Stress-strain numerical modelling performed under dynamic conditions helps to better understand the aforementioned interactions; however, these models rely on very strong constraints to reproduce the engineering geological setting of the slope and to return reliable outputs in terms of amplification functions or induced displacements (Martino, 2015).

With the goal of predicting earthquake-induced movements of landslides, possible interactions between seismic waves and slopes have been analysed in several studies (Del Gaudio and Wasowsky, 2007; Bourdeau and Havenith, 2008; Danneels et al., 2008; Lenti and

Martino, 2013) to describe how the triggering conditions depend on seismic input properties such as energy, frequency content, directivity and peak ground acceleration (PGA), as well as on the slope topography and geological setting. Some case studies (Bozzano et al., 2008, 2011; Alfaro et al., 2012; Martino et al., 2016b) highlighted the role of these interactions in response to seismic amplification effects. In particular, it was previously highlighted (Delgado *et al.*, 2011) that pre-existing large landslides can represent outliers with respect to the empirical curves of expected earthquake-triggered landslides as a function of magnitude vs. distance proposed by Keefer (1984) and Rodriguez et al. (1999), since these large pre-existing landslides can interact with far-field earthquakes characterized by long-period spectral contents.

Coseismic displacements of earthquake-triggered landslides were traditionally computed for several decades by applying the Newmark (1965) method, which considers the existing landslide mass as a rigid sliding block whose displacements are cumulated during the seismic action only in the case of PGA exceeding a threshold. Several limits were noted on the representativeness of the Newmark method in the case of nonrigid masses (i.e., in most cases of earth-slides) due to the internal deformations produced during the seismic shaking, which are responsible for amplification of the seismic motion. To consider this feature, according to a 1D resonant column model, decoupled or coupled solutions were adopted (Makdisi and Seed, 1978; Rathje and Bray, 2000) that consider the simultaneous solution of the dynamic and of the sliding analysis. Such solutions were also implemented to take into account fully nonlinear soil properties (Rathje and Bray, 2000) and to consider the probabilistic variation of the seismic input properties (Bray and Travasarou, 2007; 2009; Rathje and Antonakos, 2010).

Some recent advances in slope stability analysis as well as in coseismic displacement evaluation for pre-existing landslide masses (Del Gaudio and Wasowsky, 2011) reveal that most of the criticism in analysing the slope stability under seismic action considers the dynamic inputs for computing the safety factor (SF) and the uncertainty in assuming mechanical properties necessary for evaluating the available soil strength. On the other hand, the main criticism in computing coseismic landslide displacements depends on the rheological assumptions (i.e., rigid vs. deformable soil masses, the role of pore water pressures) and on the complexity of the physical interactions between seismic waves and landslide masses (i.e., 1D, 2D or 3D seismic amplification; incidence angle of seismic waves related to the slope geometry; seismic wave polarization within a landslide mass).

The present study addresses the role of the composite landslide mechanism that resulted in submasses divided by several secondary scarps (ascribable to multiple past reactivations) on earthquake-induced displacements. To this objective, in the framework of the European project "*MARSite – Marmara Supersite: new directions in seismic hazard assessment through focused Earth observation in the Marmara Supersite*", the large Büyükçekmece landslide located 35 km W of Istanbul (Turkey) was selected as a case study. This landslide, approximately 1500 m wide and 2200 m long, involves Upper Oligocene to Lower Miocene deposits, consisting of silty clays, tuffs and sands. It is characterized by an evident composite mechanism, responsible for several secondary scarps and counter-slope tilted terraces, which divides the landslide mass into submasses, providing them with an independent mobility.

Following the characteristic-period-based (CPB) approach recently proposed by Lenti and Martino (2013), the expected earthquake-induced displacements of the Büyükçekmece landslide were evaluated through numerical modelling, which considers the role of seismic wave properties interacting with the landslide slope.

According to the CPB approach, landslide mobility is theoretically favoured by the characteristic period of the seismic input (T_m) defined by Rathje et al. (1998), as the maximum expected earthquake-induced displacements correspond to a resonant period due to the landslide mass thickness (T_s) equal to the characteristic period (T_m) of the seismic input, which depends on the frequency content expressed by the fast Fourier transform (FFT). A characteristic period ratio of T_s/T_m was introduced by Rathje and Bray (2000) to describe such conditions, i.e., a maximum displacement is theoretically expected for a T_s/T_m ratio equal to 1. Nevertheless, the landslide mass mobility is also theoretically favoured (Hutchinson, 1994) by the characteristic period of the seismic input (T_m), which is double with respect to the period (T_l) associated with the length of the landslide mass (i.e., for a characteristic period ratio T_l/T_m equal to 0.5). According to the CPB approach, the values of the expected earthquake-induced landslide displacements depend on a combination of 1D and 2D effects, with the latter related to the more complex interactions between the landslide mass and slope geometry. In particular, for increasing the energy of the seismic input, the 2D effects become more significant, and the expected displacements are mainly related to the T_l/T_m ratio (Lenti and Martino, 2013; Martino et al., 2016b). Moreover, the 1D resonance of the landslide mass is much more evident in the case of more gentle slopes than in steeper ones (Lenti and Martino, 2012).

2. CASE STUDY

The Büyükçekmece landslide area is located in the Avcilar-Beylikdüzü peninsula (Esenyurt region), approximately 15 km north from the seismogenetic North Anatolian Fault Zone (NAF) (Kalkam, 2009) in the Marmara Sea region (Fig. 1). This area is of particular interest because it was recently struck by the 17 August 1999, M_w 7.4 Kocaeli and by the 12 November, M_w 7.2 Düzce earthquakes. Moreover, during the last decade, the urbanised area increased from 3% to 25%, covering approximately 50 km^2 with new buildings and infrastructures, while the number of inhabitants in the district increased from approximately 58000 to approximately 287000 (Maktav et al. 2000).

The Avcilar-Beylikdüzü peninsula is located at the southwestern edge of the Istanbul–Zonguldak Tectonic Unit. It is surrounded by the Istranca Metamorphic Unit in the NE (Akartuna 1953; Koral 1998), the Thrace Basin Unit in the SW, the Istanbul–Zonguldak Unit in the NNE and the young sediments of the Marmara Sea basin in the SE (Dalgiç 2004). The Istanbul–Zonguldak Unit consists of a >3000 m thick succession, which was deposited almost continuously from the Ordovician to Carboniferous periods (Packelmann 1938; Dean et al 1993; Görür et al. 1997). In the Avcilar-Beylikdüzü peninsula, the Paleozoic basement is composed of Devonian limestones, ascribable to the Trakya and to the Dolayoba Formations, which are overlaid by Oligocene to Upper Miocene sedimentary rocks.

2.1 Geological setting of the landslide slope

In the Büyükçekmece landslide area, the outcropping deposits (Fig. 2) have a subhorizontal strata attitude and can be divided into three main units: the Bakirköy member of the Çekmece Formation (Upper Miocene) consisting of alternating calcarenites, marls and clay layers (Fig. 3a); the Kiraç member of the Istanbul Formation (Upper Oligocene - Lower Miocene) consisting of sands and gravels belonging to fluvial deposits that are generally poorly or non-cemented (Fig. 3b) with rarely interbedded tuffs; and the Danisment Formation (Upper Oligocene) consisting of stiff clays and claystone-shales containing loose sand and tuff levels of different thicknesses (Fig. 3c, d).

Two fault systems can be recognized in the landslide area (Sen, 2007): the first system is NW-SE oriented and dislodges the Danisment Formation; the age of the fault system is probably pre-Upper Miocene because it does not cut the Upper Miocene deposits; the second system is NNW-SSE to WNW-ESE oriented and cuts the deposits of the Çekmece Formation. The Büyükçekmece landslide mass mainly involves the Danisment Formation and the Kiraç member of the Istanbul Formation, while the Bakirköy member of the Çekmece Formation is partially involved in the detachment area (Fig. 2). The dislodgement produced by the past landslide movements caused the Kiraç member to subside by a maximum of 50 m with respect to the corresponding plateau located E of the landslide slope.

2.2 Geomorphological features

A detailed geomorphological survey was carried out in the Büyükçekmece landslide slope using satellite images as well as collected field evidence. The surveyed landforms are ascribable to an active and complex rototranslational landslide (sensu Varnes 1978),

approximately 1500 m long and 1200 m wide, characterized by a combined mechanism with a prograding and a retrogressive style (Cruden and Varnes, 1996). This is confirmed by the collected evidence of damage to roads, buildings, walls, and infrastructures (Fig. 3e, f, g).

As observed in the longitudinal cross section (L in Fig. 2), the landslide mass is delimited upslope by a main scarp, approximately 800 m wide, and it is divided into submasses by seven secondary scarps, which originated from highly visible counter-slope tilted terraces (Fig. 3e). Each submass has a longitudinal extension of up to 300 m; the maximum vertical dislodgement of the involved deposits (ascribable to Danisment and Istanbul Formations) is up to 50 m, and it can be measured at the toe of the landslide. The tilt angle of each submass gradually varies from 30° to 40° moving downslope. The sandy deposits of the Kiraç member of the Istanbul Formation and the marly calcarenites of the Bakirköy member of the Çekmece Formation are preserved only in the two submasses of the landslide closest to the main scarp. As reported in the geological cross-section of Fig. 2, the sliding surface of the Büyükçekmece landslide has an average depth of 60 m b.g.l. in the middle and lower portion of the slope, while it decreases to 30 m b.g.l. in the upper portion of the slope. This geological setting for the landslide proves its repeated reactivations. Moreover, the distance among the single submasses is consistent with an independent mobility. Two earth flows are also evident: the first flow, approximately 450 m long and 200 m wide, is located along the left side of the rototranslational landslide mass (Fig. 3f), and the second flow, approximately 800 m long and 150 m wide, is located at its toe (Fig. 2). The total estimated volume of the Büyükçekmece landslide is approximately 140 million cubic metres, including the rototranslational mechanisms and the two earth flows.

The reconstruction of the landslide geometry and geology was also supported by several geophysical investigations (Martino et al., 2016a; Yalcincaya et al., 2016), including 5 vertical electrical sounding profiles (VES), 19 seismic noise measurements (NM), 20 seismic refraction microtremor (ReMi) profiles with MASW, and 1 borehole drilled to 70 m b.g.l. (S1 in Fig. 2). Geophysical measurements and geological field surveys in the landslide area were combined to obtain a more comprehensive engineering geological model of the site.

The resistivity values measured within the landslide mass are generally lower than 20 ohm.m, i.e., a typical value for remoulded clayey debris. A typical obtained VES profile shows a sharp increase in the resistivity values up to 100 ohm.m at almost 65 m depth below the ground level that can be related to the sliding surface. The lowest resistivity values (of almost 10 ohm.m) are generally related to the sandy deposits belonging to the Kiraç member of the Istanbul Formation. Analysis of the seismic refraction data helped reconstruct the subsurface geology up to 20 m. In the uppermost layer (up to 5 m below the ground level), P-wave velocities (Vp) are very low, on the order of 300-400 m/s, but they sharply increase locally, probably depending on the location of the water table. Regarding the S-wave velocity (Vs) profiles derived from the MASW and ReMi measurements, the penetration depth for the MASW measurements is approximately 30 m, while it reaches approximately 80 m for the ReMi measurements. Although a sharp velocity increase could be expected below the landslide mass, an almost gradual increase of velocity up to 600 m/s with depth and a minimum superficial value of approximately 150 m/s were observed. The log stratigraphy of the S1 borehole provided a depth up to 60 m b.g.l. for the main sliding surface (Fig. 2).

2.3 Monitoring system

An experimental multiparametric monitoring system was installed in the Büyükçekmece landslide at the end of October 2014 (Martino et al., 2016a), with the goal of detecting possible triggers (i.e., rainfalls and earthquakes) for landslide movement as well as measuring the rate of displacement. Due to the complexity of the landslide mass and the rototranslational mechanism involving several submasses, this system was focused on the middle slope portion of the landslide where evidence of activity and induced damages to buildings and infrastructures have been particularly intense. An in-hole installation was selected i) to constrain seismic local amplification effects related to the landslide mass (Bourdeau et al., 2017), which could facilitate its earthquake-induced mobility; ii) to detect variations in water pore pressures in a multilevel aquifer, related to both seasonal conditions (middle time-interval) and transitory effects (very short time-interval) as in the case of earthquake shaking. Since no inclinometers could be installed due to their incompatibility with the aforementioned sensors, the landslide mass mobility was detected by a superficial GPS array including two inner points and one external reference site. To install the in-hole sensors, a borehole was drilled in the S1 location (Figs. 2 and 3).

The installed monitoring system includes the following: two piezometers (vibrating wire technology) installed in the borehole to measure pore pressures at two different depths (-36 m and -51 m b.g.l.) with a measuring range of 0-2 bar, one rain gauge and a temperature sensor installed approximately 400 m SW of the borehole site, and two 3D seismic sensors

GEOSPACE 2 Hz (bandwidth ±3 dB, inherent sensitivity 2 V/in/s; sampling at 1 kHz with a threshold of 1 μm/s) installed at -45 m and -70 metres b.g.l. in the borehole.

The GPS net was installed in the landslide area recording continuous displacements at two sites inside the landslide mass (stations FM and HS of Fig. 2) and one reference site located outside in a stable area (station SC of Fig. 2). A rain gauge and temperature station were also installed in correspondence to the GPS station HS.

In particular, this net consisted of a GPS-RTK system based on technologies of differential GPS, and each station is designed for periodic 3D displacement measurements with a precision up to a couple of centimetres. The signals were transmitted wirelessly, and the measurement corrections were transmitted to GPS measurement devices in the field, offering much better precision in the assessment of displacements. To this objective, the radio antenna of each GPS station had a reasonable line of sight to the reference station and a distance of less than 1 km.

The GPS differential measurements output a continuous movement of the landslide mass in the longitudinal direction (WE), i.e., consistent with the kinematic direction of the landslide, with an average rate of almost 2 cm/month (Fig. 4). Based on these data and according to the velocity scale proposed by Cruden and Varnes (1996), the Büyükçekmece landslide can be defined as a slow to very slow phenomenon. The use of Landsat satellite images (available during the time interval 1984-2013) was considered in the frame of the MARSite project; nevertheless, the data show a notable increase in the urbanised area, especially inside the landslide areas as confirmed by satellite optical images (Fig. 5), which limits the capability to

detect landslide mobility. In addition, many anthropic deposits or excavations performed during the last decade significantly changed the topographic shape, thus creating unreliable change detection analyses.

Fig. 4 reports a synoptic view of the sensors, including piezometer data and rainfall intensities, monitoring the GPS cumulative differential displacement at station FM using rainfall intensity and the GPS cumulative differential displacement at station FM using the PGA distribution for 65 earthquakes recorded by the 3D seismic sensors at the S1 borehole. Due to technical problems, the measuring system operated regularly only until May 2015. As reported in Fig. 4, several sensors did not record any data in the following months.

2.4 **Hydrogeological model**

A hydrogeological model of the Büyükçekmece landslide mass was reconstructed mainly based on field evidence, and it was compared with the one-year data recorded by the two piezometers installed in the S1 borehole. According to the hydrogeological model, the groundwater circulation in the landslide slope is related to two different flow nets: the first flow net is perched in the sandy deposits of the Kiraç member and in the tuff of the Danisment Formation (corresponding to the pore pressure recorded at -36 m b.g.l. and ranging between 290 and 320 hPa), and the second flow net is located in the landslide mass debris above the sliding surface (corresponding to the pore pressure recorded at -51 m b.g.l. and ranging from 360 to 420 hPa). Since the piezometric data have been available only for one year (from October 2014 to October 2015), they show that a seasonal trend exists in the pore water pressures (u(t)) recorded at the -51 m piezometer, while a more irregular trend

characterizes the -36 m piezometer, which seems mostly related to rainfall events (Fig. 4). No evident relationship is currently recognized between the u(t) and the rate of displacement recorded for the WE component of the landslide movement by the GPS monitoring system. Moreover, based on the available data, no relationship can be easily deduced between pore pressures, displacements and earthquake occurrence comparing the cumulative curves of rainfall events and u(t) with (Fig. 4b) the PGA distribution of the recorded earthquakes (Fig. 4a).

Based on the geological setting of the slope, three hydrogeological units were distinguished as follows: 1) the aquifer (including the Kiraç member of the Istanbul Formation and the Bakirköy member of the Çekmece Formation); 2) the aquitard (including the tuff levels of the Danisment Formation); and 3) the aquiclude (corresponding to the claystone-shales of the Danisment Formation). Moreover, using a remote detection by satellite images coupled with survey observations, several spring points were recognized, which generally correspond to pool zones, where evidence of superficial water can be collected during the year. It is considered a main contribution to the water circulation within the landslide from the plateau area, located E of the slope, and a reduced contribution from the ridge located along the right side (Fig. 6). Such assumptions are derived from the following considerations: i) the geometrical features of the ridge zones separating the landslide form the adjacent slopes, ii) the attitude of the permeability contacts is another consideration, iii) the recognized spring points are another consideration, the general trend of the flow net in the landslide slope results in a SE-NW direction, iv) springs are evident only on the left side of the landslide, v) an earthflow originates from the left side of the landslide, vi) a lateral contact exists between the

tuff and the clay of the Danisment Formation due to the NNW-SSE oriented fault on the left side of the landslide, and vii) several spring points are distributed in the middle portion of the landslide mass and are located along the secondary scarps.

Surface water runoff paths (Fig. 7) suggest that a hydraulic connection exists among the dislodged hydrogeological units that constitute the landslide submasses. In particular, a more likely explanation is that the scheme of superficial water circulation is referred to a racking system, which provides a seasonal connection among the aquifer hosted in the plateau and the ones hosted in the dislodged submasses (Fig. 7a). When the water levels fall below the racking thresholds (i.e., the permeability contact between aquitard and aquiclude) no connections exist among the dislodged submasses (Fig. 7b).

The piezometer records prove that the shear zone of the landslide hosts a groundwater flow directly fed by the plateau aquifer (Fig. 7c). Nevertheless, based on the geological setting of the slope, it is admissible that a seasonal contribution to this flow is derived from the minor aquifer hosted in the submasses closest to the main scarp, which are directly connected to the aquifer hosted in the plateau (Fig. 7d).

According to the hydrogeological model proposed here, in the Büyükçekmece landslide, the maximum hydraulic head of the superficial aquifer is regulated by levels of racking thresholds, while the hydraulic head of the deeper water circulation depends on the recharge of the aquifer in the plateau. The hydraulic head of the deeper water circulation is approximately 5 m, as it results from the piezometric measurements at the S1 borehole site, while the seasonal

oscillation of the water pressures recorded to date are very limited since they do not exceed 1 m.

3. SLOPE STABILITY

The slope stability conditions of the Büyükçekmece landslide were analysed by the global limit equilibrium (GLE). To this aim, for the slice approach, the simplified method by Bishop (1955) was selected for the following reasons: i) the complex setting of the landslide, including several submasses, does not allow a valid assumption of the GLE approach by Janbu (1973) because the interslice shear force distribution cannot be assumed colinear and the related Janbu's correction factor is unreliable; ii) the use of the more simple and more traditional method by Fellenius (1927) would have neglected the lateral interslice strength, thus introducing a stronger approximation due to the submass dislodgement of the landslide; iii) a purely translational mechanism is incorrect since the counter-slope tilting of the landslide submasses demonstrates that important rotational components of the sliding mechanism exist; and iv) double convergence methods (e.g., Morgestern and Price, 1965) would introduce large uncertainties in parameter values due to the complexity of the slope geological setting, and a unique mass equilibrium could not be analysed in any case.

To apply Bishop's method in case of impure rotational sliding, the Büyükçekmece landslide mass was split into submasses having a more or less circular sliding surface with a radius dimension that justifies the counter-slope tilt angle of each submass along the geological cross section L in Fig. 2. These derived submasses are delimited by sliding surfaces with an error

lower than 25 m with respect to the actual shape of the sliding surface. The aforementioned limitations due to Bishop's method, which was performed on submasses, can affect the computed values of the SF more than their qualitative distribution inside the landslide mass (i.e., moving from the stable plateau down to the landslide toe).

Seven sliding surfaces (sl1 to sl7 in Fig. 2) were considered from the top to the bottom of the slope, with the first surface corresponding to the main sliding surface (i.e., enveloping the whole landslide mass). According to Bishop's method, the submasses were split in slices and a safety factor was computed in the form:

$$SF = \sum [[c_j b_j + (W_j (1-r_u) tg\psi_j))]m_i]/\sum[W_j(\sin\alpha_j + k_x(x_j)dx_j/R)] \quad (1)$$

where j is the number of slices, α is the slice inclination, dx is the arm of the $Wk_x(x)$ force with respect to the centre of the sliding surface, R is the radium of the sliding surface, c is the cohesion, W is the weight force, ψ is the internal friction angle, r_u is the pore water pressure coefficient according to Bishop (1955), and m is a trigonometric coefficient from the equation:

$$m_j = [\cos\alpha_j + (\sin\alpha_j \tan\psi_j/SF)]^{-1} \quad (2)$$

A sensitivity analysis was also performed to obtain the SF distribution for r_u varying from 0 (dry conditions) to the maximum admissible values (0.5) as well as for the pseudostatic coefficient, k_x, varying from 0 to 0.4 g. In this regard, it is worth noting that a PGA of 0.35 g is representative for an expected earthquake with a 475 yr return time focused along the NAF (Erdik et al. 1999; Atakan et al. 2002).

The mechanical properties requested by the GLE analysis according to equation (1) were attributed from literature data (Cetin et al. 2004; Dalgiç 2004) and are summarized in Table 1. The stability chart, which reports the critical values of the pseudostatic coefficient k_c vs. r_u for each sliding surface (i.e., the main and the secondary surfaces), indicates that the stability conditions increase from the plateau to the landslide toe. In particular, relevant differences in the $k_c(r_u)$ distributions only result for surfaces sl5 and sl6 located down slope (Fig. 8). On the other hand, sliding surfaces sl7 and sl8 remain in stable conditions within the considered ranges of the k_c and r_u values. It is worth noting that, due to the maximum water pressure measured in the S1 borehole along the sliding surface, an r_u up to 0.04 accounts for regular ground water flow conditions. According to the stability chart, in these conditions, a k_x value higher than 0.4 g (i.e., a return period within the range of 475-2475 yr according to Erdik et al., 1999) should be invoked for causing the landslide reactivation.

4. DYNAMIC NUMERICAL MODELLING OF EARTHQUAKE-INDUCED DISPLACEMENTS

Expected earthquake-induced displacements of the Büyükçekmece landslide were computed through a dynamic stress-strain numerical model performed along the longitudinal section L in Fig. 2 by the 2D finite difference code FLAC 7.0 (Itasca 2011).

The landslide area was divided into quadrilateral zones, providing an accurate representation of the wave transmission through the model up to 10 Hz (Kuhlemeyer and Lysmer, 1973).

The parameters used for modelling are reported in Table 1. On the basis of the performed geophysical investigations (Martino et al., 2016), a variation of parameter values was also accounted for, depending on the submass position and depth. In particular, a linear increment of stiffness was attributed to the landslide substratum (according to the measured Vs) and a gradually decreasing stiffness was considered for each geomechanical unit, moving from top to bottom on the slope (i.e., for each submass of the landslide). Based on the material properties (in particular, the minimum shear-wave velocity Vs) and the frequency content of the input motions (in particular, the maximum frequencies), the numerical domain was discretized in an approximately 2-3 m sized mesh, resulting in 107200 nodes (800 along the x direction and 134 along the y direction, respectively). Absorbing quiet boundaries (Kuhlemeyer and Lysmer, 1973) and free field boundaries (Cundall et al., 1980) were applied along the base and the lateral boundaries of the model, respectively, to prevent the reflection of outward propagating waves back into the numerical domain. A visco-plastic rheology was applied to the landslide mass deposits, and a visco-elastic rheology was applied to the landslide substratum. Energy dissipation was solved by a Rayleigh damping function, which is frequency-independent over a restricted range of frequencies (Itasca, 2011). A critical damping ratio equal to 2% was used for the landslide mass only, and 0.5% was used elsewhere.

4.1 Seismic inputs

Seismic inputs were applied in the form of a vertically upward propagating SV stress wave at the base of the model. To follow the CPB approach, the inputs were derived by selecting 12 accelerometric records of the European database integrated with records from the K-NET and COSMOS databases (Table 2). They are characterized by Arias intensity (AI) values on the order of 0.01 m/s and by different values of the characteristic period, T_m, ranging from 0.2 to 16.5 s. Depending on the proper landslide dimensions, the computed T_s is equal to 0.82 s, while T_l is equal to 6.22 s. As a consequence, the values of the T_s/T_m ratio are in the range of 0.05–4.29, while the values of the T_l/T_m ratio are in the range of 0.38–32.72.

To perform the landslide mobility analysis, the time histories of the selected inputs were scaled to have AI values of 0.001 and 1 m/s without modifying the T_m; in this way, 36 inputs were available, representative of three energy levels in a wide range of T_m values. Moreover, to perform the dynamic modelling, an equivalent signal was associated with each selected input according to the LEMA_DES (Levelled-Energy Multifrequential Analysis for deriving Dynamic Equivalent Signals) approach by Lenti and Martino (2010). The LEMA_DES procedure generates a sequence of functions and signals that produce a resulting multifrequential dynamic equivalent input that is energy-equivalent to the reference signal, best-fitted in terms of the PGA via an iterative procedure performed on the number of equivalent cycles and with a time duration that is significantly shorter than that of the reference signal. The use of this approach in dynamic numerical modelling guarantees the following (Lenti and Martino, 2010): i) checking that the frequency content of the derived signals is defined within a representative/admissible range; ii) avoiding exceeding the upper-threshold frequency during modelling; iii) narrowing the energy gap between the real and

simulated seismic actions; iv) controlling the maximum intensity of the adopted action; and v) reducing the computational time (especially in the case of parametric analyses, where a high number of iterations are requested), as the equivalent input is typically shortened with respect to the reference.

4.2 Numerical modelling

To account for possible effects due to the composite mechanism of the landslide, i.e., to the dislodgements of the whole landslide volume in several submasses, two numerical models were designed: the first model considers the real heterogeneities related to the complex geological setting of the landslide; the second model assumes a very simplified condition, characterized by a homogeneous composition of the landslide mass. In the second model, the claystone-shales of the Danisment Formation were considered for the whole landslide mass composition.

To take into account the water circulation capable of influencing the landslide movement, two hydraulic conditions were modelled by generating water tables (i.e., adopting a pseudostatic solution), which solves the initial equilibrium considering effective stresses. The first hydraulic condition reproduces the pore pressures above the main sliding surface of the landslide that are only related to deep-water circulation (Fig. 7b). The second hydraulic condition reproduces the possible interactions between the superficial and the deep-water circulation, admissible in some seasonal conditions when the increase in the pore pressure up to the racking threshold could occur in the submasses that are closest to the main landslide scarp (Fig. 7c).

The obtained results were plotted on graphs showing the horizontal displacements (x-disp) computed for each applied input, which correspond to the characteristic ratios of T_s/T_m and T_l/T_m. These distributions indicate the roles of both the 1D resonance and the 2D input-slope interaction in the induced landslide displacements. According to Lenti and Martino (2013), the x-disp values were computed by averaging the largest displacements referred to different percentages of the grid nodes within the landslide mass in the numerical domain.

For each considered level of AI, Newmark's displacement was computed by the empirical approach of Hsieh and Lee (2011), considering the worldwide curves for soil site in the form:

$$\log D_N = 0.802 \log AI - 10.981\, k_c(r_u) + 7.377\, k_c(r_u) \log AI + 1.914 \pm 0.274 \quad (3)$$

where D_N (in cm) is Newmark's displacement, AI (in m/s) is the Arias intensity, $k_c(r_u)$ is the pseudostatic critical coefficient for a Bishop coefficient (r_u) value. Taking into account the hydraulic conditions assumed for the Büyükçekmece landslide, the D_N values were computed assuming r_u equal to zero and a result lower than 10^{-1} cm for each considered AI value.

The local seismic response of the landslide site was previously studied though numerical modelling supported by geophysical investigations by Bourdeau et al. 2017. The obtained results demonstrate that the complex geological setting of the landslide slope is responsible for a local seismic response characterized by a wide range of amplified frequencies. In particular, the landslide area is characterized by higher resonance frequencies than outside zones, and relevant amplifications are expected at frequencies between 2 and 4 Hz. These amplifications can be related to the impedance contrast between the Büyükçekmece landslide

mass and the local substratum (i.e., seismic bedrock), while no significant topographic effects were output by modelling the propagation of seismic waves into the slope.

The seismic wave propagation obtained by the numerical modelling in the landslide slope (Figs. 9, 10) demonstrates that there is no reflection of outward propagating waves back into the model due to the correct efficiency of the lateral quiet boundaries. Moreover, for increasing values of AI, more intense superficial seismic waves are generated within the landslide mass. Such an effect is much more evident in the case of a heterogeneous landslide mass (Fig. 9) with respect to a homogeneous case (Fig. 10). This result indicates the key role played by the geological setting of the landslide and, in particular, by the dislodgement in submasses, which is derived from multiple mechanisms.

5. DISCUSSION

The numerical modelling results for the Büyükçekmece landslide also show that, in the case of real heterogeneous conditions (Fig. 11), the maximum earthquake-induced displacements vary from 1.5 cm to 15 cm for AI values ranging from 0.01 to 1 m/s. Therefore, for AI values equal to 1 m/s, the computed x-disp values vary from 0.05 m to 0.1 m for the percentage of grid nodes ranging from 5% to 100% while in the same percentage range, they vary from 0.005 m to 0.01 m for AI values equal to 0.01 m/s. In any case, the obtained displacements are higher than Newmark's displacements. Regarding the characteristic period ratios, it is worth noting that in the heterogeneous conditions, the maximum displacement occurs for a T_s/T_m ratio close to the critical AI value of 1 to 0.1 m/s. This agrees well with the evidence

discussed by Bourdeau et al. (2017) involving local seismic amplification related to the impedance contrast between the landslide mass and its substratum. Nevertheless, for AI values higher than 0.1 m/s, the maximum displacements do not occur for any critical value of T_s/T_m and T_l/T_m. This behaviour is independent of the considered percentage for the grid nodes.

If a homogeneous composition of the landslide mass is assumed (Fig. 12), the x-disp value varies from 0.01 to 1 m for AI values ranging from 0.01 to 1 m/s. In this case, the maximum x-disp values occur for a T_s/T_m ratio equal to 1 in the case of an AI value less than 1 m/s and for a T_l/T_m ratio equal to 0.5 in the case of higher AI values; thus, significantly higher respect is given to the Newmark's displacements and to the displacements computed in heterogeneous conditions. Moreover, for an AI value equal to 1 m/s, the computed x-disp values vary from 0.07 m to 1 m for the percentage of the grid nodes ranging from 5% to 100% while in the same percentage range, they vary from 0.005 m to 0.01 m for an AI value equal to 0.01 m/s. This means that, in the case of a simplified assumption about the landslide mass composition, the theoretical conditions for expecting maximum displacements related to 1D and 2D interactions of seismic waves with the landslide are fully satisfied (Lenti and Martino (2013). In contrast, the heterogeneous conditions, referring to a more realistic composition of the landslide mass, do not verify the abovementioned theoretical conditions, especially in the case of high AI values when a critical T_l/T_m ratio equal to 0.5 should be expected for the maximum landslide mobility. It is worth noting that the difference between the distributions of x-disp vs. characteristic period ratios, computed for the heterogeneous and the homogeneous landslide masses, increases with increasing AI values. This is consistent with

the more intense interactions between seismic waves and the landslide mass shown in the propagation maps of Figs. 9 and 10.

To provide a reliable explanation for such a finding, a T_l^* was computed with respect to the average length of a single submass of the landslide (130 m), i.e., delimited by secondary scarps, which results in approximately 0.36 s. The obtained distribution of the x-disp vs. T_l^*/T_m ratio (Fig. 11) reveals that maximum displacements occur for the theoretical critical value of 0.5 in the case of AI values higher than 0.1 m/s and for a T_s/T_m value equal to the theoretical value of 1 for lower AI values. Therefore, the Büyükçekmece landslide mobility is strongly conditioned by its composed rototranslational mechanism, which generated the dislodgement of the landslide in several counter-slope tilted submasses, thus reducing the characteristic period T_l. This means that the evolution of landslides in the case of multiple phases of activity can significantly modify the interaction of their masses with the seismic waves over time by reducing the characteristic period T_l because of increasing dislodgement or fragmentation in the submasses. This induces shortening of the characteristic period T_m for earthquakes, which can be responsible for the maximum landslide mobility.

Further numerical modelling was carried out considering the WE component (i.e., in the landslide sliding direction) of the seismic input specifically obtained in the framework of the MARSite project by Aochi et al. (2016) for the Büyükçekmece landslide site (28.6678°E, 40.9908°N), representative of a seismic scenario corresponding to a return period of 475 yr and a Mw=7.05. This input was obtained performing numerical simulations of dynamic rupture processes along the NAF in the Sea of Marmara, and the following was considered: i)

adopting a 3D finite difference code, ii) taking into account the 3D structure around the Sea of Marmara, and iii) including the bathymetry and the sea layer. Simulations were carried out (Aochi and Ulrich, 2015) for different earthquakes (moderate point sources and large finite sources) to provide shake maps to study the variability of ground-motion parameters as well as to provide synthetic seismograms for the blind inversion tests.

Starting from the time history of the input (shown in Fig. 13 and available at http://aochi.hideo.perso.neuf.fr/), the equivalent LEMA_DES signal was derived, characterized by an AI value on the order of 0.1 m/s and a T_m value of 0.8 (Fig. 13). The modelled x-disp values are in very good agreement with the distribution of x-disp values vs. characteristic period ratios obtained here according to the CPB approach. In particular, the displacements result in the same order of magnitude for 5% of the grid nodes, while they are coincident if 100% of the grid nodes are considered.

The role of water circulation in the landslide mass was also accounted for by considering the two abovementioned hydraulic conditions. Nevertheless, no relevant differences resulted in the x-disp vs. characteristic period distributions by modelling the effective stress conditions (i.e., considering the two assumed water tables) with respect to the total stress conditions. These results demonstrate the negligible effect of steady water pressures (and corresponding effective stresses) in the earthquake-induced displacements expected for the Büyükçekmece landslide. Although it cannot be excluded that coseismic overpressures generated within the landslide mass could affect the resulting displacements, no reliable constitutive laws were implemented, especially in the case of coherent soils, for solving fully nonlinear dynamic

behaviour by finite difference methods that allow the modelling of transient effective stress conditions.

6. CONCLUSIONS

Earthquake-induced landslide mobility is significantly conditioned by 1D and 2D interactions with seismic waves propagating within the landslide mass. The present study focuses on the Büyükçekmece landslide (approximately 1500 m wide and 2200 m long), located in Turkey, W of Istanbul, approximately 15 km northward from the NAF. The results obtained by modelling the composite landslide mass and its hydrogeological conditions using a finite difference numerical code confirmed the role of characteristic periods related to landslide length and depth (T_l and T_s, respectively) and to the earthquake characteristic period (T_m) in providing distributions of expected displacements. Nevertheless, this case study indicated the relevant role of the landslide mass heterogeneity. A composite rototranslational mechanism was responsible for the dislodgement of the landslide mass into submasses, reducing the characteristic period T_l related to the landslide length. In particular, the reduced T_l value implies a more efficient interaction of the dislodged landslide mass with earthquakes characterized by shorter periods, T_m. As a result, the evolution of landslides could modify their interactions with seismic waves in the case of multiple phases of activity as it can induce a change over time for the T_l value due to increasing dislodgement or fragmentation of the landslide mass. The quantitative results obtained by the dynamic numerical modelling reported here indicate the relevance of an earthquake-induced landslide reactivation

corresponding to a return period of 475 yr and a Mw=7.05, since the expected displacements (2–4 cm) are comparable to those cumulated by the continuous landslide movement over one year (considering the measured rate of approximately 2 mm/month), which can produce evident and intense damages to buildings and infrastructures.

AKNOWLEDGEMENTS

The study was carried out in the framework of the *MARSite* (*Marmara Supersite: new directions in seismic hazard assessment through focused Earth observation in the Marmara Supersite*, grant agreement n°: 308417 of the 7th Framework Programme). More in particular, the here reported research was carried out as part of the WP6 "Earthquake-induced Landslide Hazard in Marmara". The authors wish to thank Danilo D'Angiò and Antonella Sacco for their contributions to data processing and geological mapping.

REFERENCES

Akartuna, M., 1953. Geology of Catalca-Karacaköy Region (in Turkish). Istanbul University. Fen Fakültesi Monografi serisi, 13.

Alfaro, P., Delgado, J., Garcia-Tortosa, F.J., Giner, J.J., Lenti, L., Lopez-Casado, C., Martino, S., Scarascia Mugnozza, G., 2012. The role of near-field interaction between seismic waves and slope on the triggering of a rockslide at Lorca (SE Spain). *Natural Hazards and Earth System Sciences*, 3631-3643.

Aochi, H., Ulrich, T., 2015. A Probable Earthquake Scenario near Istanbul Determined from Dynamic Simulations, Bulletin of the Seismological Society of America, 105(3), 1468–1475.

Aochi, H., Ulrich, T., Douglas, J., 2016. Ground motion simulations in Marmara (Turkey) region from 3D finite difference method. Geophysical Research Abstracts. Vol. 18, EGU2016-2262.

Atakan, K., Ojeda, A., Meghraoui, M., Barka, A.A., Erdik, M., Bodare, A., 2002. Seismic Hazard in Istanbul following the 17 August 1999 Izmit and 12 November 1999 Düzce Earthquakes. Bulletin of the Seismological Society of America 92(1), 466–482.

Bishop, A.W., 1955. The use of the slip circle in the stability analysis of slopes. Géotechnique 5(1):7–17.

Bourdeau, C., Lenti, L., Martino, S., Ozel, O., Yalcinkaya, E., Bigarrè, P., Coccia, S., 2017. Comprehensive analysis of the local seismic response in the complex Büyükçekmece landslide area (Turkey) by engineering-geological and numerical modelling. Engineering Geology, 218, 90–106.

Bourdeau, C., Havenith, H.B., 2008. Site effects modeling applied to the slope affected by the

Suusamyr earthquake (Kyrgyzstan, 1992). Engineering Geology, 97, 126-145.

Bozzano, F., Lenti, L., Martino, S., Paciello, A., Scarascia Mugnozza, G., 2008. Self-excitation process due to local seismic amplification responsible for the reactivation of the Salcito landslide (Italy) on 31 October 2002 Journal of Geophysical Research, 113, B10312.

Bray, J.D., Travasarou, T., 2007. Simplified procedure for estimating earthquake-induced deviatoric slope displacements, J. Geotech. Geoenviron. Eng. 133(4), 381–392.

Bray, J.D., Travasarou, T., 2009. Pseudostatic Coefficient for Use in Simplified Seismic Slope Stability Evaluation: Journal of Geotechnical and Geoenvironmental Engineering, 135, 1336- 1340.

Cetin, K.O., Isik, N., Unutmaz, B., 2004. Seismically induced landslide at Degirmendere Nose, Izmit Bay during Kocaeli (Izmit)-Turkey earthquake. Soil Dynamics and Earthquake Engineering 24:189–197.

Cruden, D.M., Varnes, D.J., 1996. Landslide types and processes, in Landslides: Investigation and Mitigation, A. K. Turner and R. L. Schuster (Editors), Transportation Research Board, Spec. Report 247, National Research Council, National Academy Press, Washington, DC, 36–75.

Cundall, P., Hansteen, E., Lacasse, S., Selnes, P.B., 1980. NESSI, soil structure interaction program for dynamic and static problems. Norges Geotekniske Institute, Norway, Report 51508-9.

Dalgiç, S., 2004. Factors affecting the greater damage in the Avcılar area of Istanbul during the 17 August 1999 Izmit earthquake. Bull Eng Geol Env 63:221–232.

Danneels, G., Bourdeau, C., Torgoev, I., Havenith, H.B., 2008. Geophysical investigation and

dynamic modeling of unstable slopes: case-study of Kainama (Kyrgyzstan). Geophysical Journal International, 175(1), 17–34.

Dean, W., Martin, F., Monod, O., 1993. Report on Field Programme with Turkish Petroleum Company in Northern and Southern Turkey (1990–1992). Turkish Petroleum Corporation (TPAO) Report AG (ed) Regional and petroleum geology of the Black Sea and surrounding region. Am Assoc Petrol Geol Mem 68:138–226.

Del Gaudio, V., Wasowski, J., 2007. Directivity of slope dynamic response to seismic shaking. Geophys. Res. Lett 34, L12301, doi:10.1029/2007GL029842.

Del Gaudio, V., Wasowski, J., 2011. Advances and problems in understanding the seismic response of potentially unstable slopes. Engineering Geology, 122, 73–83.

Delgado, J., Peláez, J.A., Tomás, R., García-Tortosa, F.J., Alfaro, P., López Casado, C., 2011. Seismically-induced landslides in the Betic Cordillera (S Spain). Soil Dynamics and Earthquake Engineering, 31, 1203–1211.

Erdik, M., Biro, Y.A., Onur, T., Sesetyan, K., Birgoren, G., 1999. Assessment of earthquake hazard in Turkey and neighboring regions. Annali di Geofisica 42:1125-1138.

Fellenius, W., 1927. Erdstatische berechnungen. W. Ernst und Sohn, Berlin.

Fotopoulou, S.D., Pitilakis, K.D., 2015. Predictive relationships for seismically induced slope displacements using numerical analysis results. Bull Earthquake Eng, 13, 3207–3238

Görür, N., Monod, O., Okay, A., Sengör, A.M.C., Tüysaz, O., Yigitbas, E., Sakinc, M., Akkök, R., 1997. Palaeogeographic and tectonic position of the Carboniferous rocks of the Western Pontides (Turkey) in the frame of the Variscan belt. Bull Soc Ge´ol Francia 168:197–205

Hsieh, S.U., Lee C.T., 2011. Empirical estimation of the Newmark displacement from the Arias intensity and critical acceleration. Engineering Geology, 122, 34-42.

Hutchinson, J. N., 1994. Some aspects of the morphological and geotechnical parameters of landslides, with examples drawn from Italy and elsewhere, Geologica Romana, 30, 1–14.

ITASCA, 2011. FLAC 7.0: User manual, Licence number 213-039-0127- 18973, Sapienza-University of Rome, Earth Science Department.

Janbu, N., 1973. Slope stability computations. In: Embankment Dam Engineering, Casagrande Memorial Volume. Wiley, New York, 47-86.

Kalkan, E., Gülkan, P., Yilmaz, N., Çelebi, M., 2009. Reassessment of Probabilistic Seismic Hazard in the Marmara Region. BSSA, 99, 2127-2146.

Keefer, D.K., 1984. Landslides caused by earthquakes. Geol. Soc. Am. Bull., 95, 406-421.

Koral, H., 1998. Progressive Mid-Tertiary geometry of a major crustal fault in the southeastern Strandjha massif. 12th Petroleum Congress and Exhibition of Turkey, Metu Convention Center, Ankara.

Kuhlemeyer, R.L., Lysmer, J., 1973. Finite element method accuracy for wave propagation problems. J. Soil Mech. Found, Div. ASCE, 99(SM5), 421-427.

Lenti, L., Martino, S., 2010. New procedure for deriving multifrequential dynamic equivalent signals (LEMA_DES): a test-study based on Italian accelerometric records, Bulletin of Earthquake Engineering, 8, 813-846.

Lenti, L., Martino, S., 2012. The interaction of seismic waves with step-like slopes and its influence on landslide movements. Engineering Geology, 126, 19-36.

Lenti, L., Martino, S., 2013. A Parametric Numerical Study of Interaction between seismic waves and landslides for the evaluation of the susceptibility to seismically induced displacements. Bull. Seism. Soc. Am., 103(1), 33.56.

Makdisi, F.I., Seed H.B., 1978. Simplified procedure for estimating dam and embankment earthquake-induced deformations. J. Geotech. Engrg. Div., ASCE, 104(7), 849–867.

Maktav, D., Sunar, F., Taberner, M., Akgün, H. 2000. Monitoring urban expansion in the Büyükçekmece district of Istanbul using satellite data. International Archives of Photogrammetry and Remote Sensing XXXIII, parte B7, Amsterdam 2000.

Martino, S., Bigarrè, P., Bourdeau, C., Coccia, S., Lenti, L., Ozel, O., Yalcinkaya, E., 2016a. Integrated engineering-geological and numerical approach applied to the large Büyükçekmece (Turkey) landslide for evaluating earthquake-induced effects. Proc. XI International Symposium on Landslides. Landslides and Engineered Slopes. Experience, Theory and Practice, Aversa et al. (Eds), Associazione Geotecnica Italiana, Rome, Italy, ISBN 978-1-138-02988-0

Martino, S., Lenti, L., Delgado, J., Garrido, J., Lopez Casado, C., 2016b. Application of a Characteristic Periods-Based (CPB) approach to estimate earthquake-induced displacements of landslides through dynamic numerical modelling. Geophys. J. Int. doi: 10.1093/gji/ggw131.

Martino, S., 2015. Earthquake-induced reactivation of landslides: recent advances and future perspectives. In: Sebastiano D'Amico. Earthquakes and Their Impact on Society. p. 291-322, Springer International Publishing AG Switzerland, ISBN: 978-3-319-21752-9, doi: 10.1007/978-3-319-21753-6_10.

Morgestern, N.R., Price, VE., 1965. The analysis of the stability of general slip surfaces. Geotechnique, 15(1), 79-93.

Newmark, N.M., 1965. Effects of earthquakes on dams and embankments. Geotechnique

15(2), 139–159.

Packelmann, W., 1938. Neue Beitrage zur Kenntnis der Geologie, Palaontologie und Petrographie der Umgegend von Konstantinopel. Abhanlundgen der Preussischen Geologischen staatsanstalt. I Neue Folge 186

Rathje, E.M., Antonakos, G., 2010. Recent advances in predicting earthquake-induced sliding displacements of slopes, in Proc. Fifth International Conference of Recent Advances in Geotechnical Earthquake Engineering and Soil Dynamics, May 24–29, San Diego, California, 1–9.Rathje, E.M., Abrahamson, N.A., Bray, J.D., 1998. Simplified frequency content estimates of earthquake ground motions. J. Geotech. and Geoenvir. Eng., ASCE, 124(2), 150–159.

Rathje, E.M., Bray, J.D., 2000. Nonlinear Coupled Seismic Sliding Analysis of Earth Structures. Journal of Geotechnical and Geoenvironmental Engineering, ASCE, 126(11), 1002-1014.

Rodriguez, C.E., Bommer, J.J., Chandler, R.J., 1999. Earthquake-induced landslides: 1980-1997. Soil Dynamic Earthquake Engineering, 18, 325-346.

Sen, S., 2007. A fault zone cause of large amplification and damage in Avcılar (west of Istanbul) during 1999 Izmit earthquake. Nat. Hazards, 43, 351–363.

Varnes, D.J., 1978. Slope movement types and processes. In: Schuster R.L. & Krizek R.J. (Eds.), Special Report 176 Landslides: Analysis and Control. Transportation Research Board, National Research Council, Washington D.C., 11-33.

Yalcinkaya, E., Alp, H., Ozel, O., Gorgun, E., Martino, S., Lenti, L., Bigarrè, P., Coccia, S.

2016. Near-surface geophysical methods for investigating the Buyukcekmece landslide in Istanbul, Turkey. Journal of Applied Geophysics, 134, 23-35.

Fig. 1 – Location of the Büyükçekmece landslide in the Sea of Marmara region. The NAF and the epicentre of the 1999 Kocaeli and Düzce earthquakes are also indicated.

Fig. 2 – Geological and geomorphological map of the Büyükçekmece landslide: 1) alluvial and coastal deposits (Holocene); 2) silty-clays of the Danisment Formation (Upper Oligocene); 3) clays with tuffs in the Danisment Formation (Upper Oligocene-Lower Miocene); 4) sands and gravels of the Istanbul Formation - Kiraç member (Upper Oligocene-Lower Miocene); 5) calcarenites of the Çekmece Formation - Bakirköy member (Upper Miocene); 6) earthflow debris; 7) rototranslational landslide mass; 8) slope debris; 9) landslide counter-slope tilted terrace; 10) rototranslational landslide scarp; 11) earthflow crown; 12) supposed fault; 13) S1 borehole; and 14) GPS station. The geological cross-section along trace L is also reported.

Fig. 3 – Photographs of the Büyükçekmece landslide area: a) stratigraphic contact between the Bakirköy member (*bk*) of the Çekmece Formation (Upper Miocene) and Kiraç member (*ky*) of the Istanbul Formation (Upper Oligocene – Lower Miocene) in the plateau zone, east of the landslide slope; b) sands and gravels belonging to the Kiraç member of the Istanbul Formation (Upper Oligocene – Lower Miocene); c) silty-clay with tuff levels in the Danisment Formation (Upper Oligocene); d) claystones of the Danisment Formation (Upper Oligocene); e) panoramic photograph of the Büyükçekmece landslide detachment area, including the main terrace and one of the secondary scarps (location of the S1 borehole is also shown); f) detachment area of the

earthflow at the left side of the landslide; and g) evidence of a counter-slope tilted terrace within the landslide mass and damage to a building due to the landslide activity.

Fig. 4 – Synoptic graph reporting the records of the monitoring system installed in the Büyükçekmece landslide area. a) Sequence of u(t) and daily rainfall; b) cumulative rainfall amounts and differential GPS displacements at station FM; and c) PGA of the earthquakes in the S1 borehole and differential GPS displacements at station FM.

Fig. 5 - Google Earth satellite images clearly showing the increase in the urbanisation in the area affected by the Büyükçekmece landslide, contoured by the black line, during the decade of 2002-2012.

Fig. 6 – Geological map of the Büyükçekmece landslide with the deduced direction of water flow and the location of the spring points. See Fig. 2 for the geological legend.

Fig. 7 –Sketches of the hydraulic conditions deduced from the hydrogeological model of the Büyükçekmece landslide. Superficial water circulation: a) perched aquifers within the landslide submasses in isolated conditions, b) perched aquifers when a connection exists due to seasonal recharge from the plateau, and c) water level of the perched aquifers seasonally limited by the permeability threshold and consequent formation of a spring point. Deep water circulation: d) water flow along the sliding surface fed by the plateau aquifer and e) water level assumed along the sliding surface in the pseudostatic hydraulic model due to the seasonal connection between the superficial and the deep circulation. See Fig. 2 for the geological legend.

Fig. 8 – Stability chart obtained by the GLE Bishop's analysis for main and secondary sliding surfaces reported in Fig. 2.

Fig. 9 – Seismic wave propagation in the numerical model by considering a heterogeneous landslide mass (input used: ID#12 in Table 2). Key to legend: 1) claystones of the Danisment Formation, 2) sands and gravels of the Kiraç member of the Istanbul Formation, 3) calcarenites and marls of the Bakirköy member of the Çekmece Formation, 4) slope debris, 5) sliding surfaces, and 6) fault.

Fig. 10 – Seismic wave propagation in the numerical model by considering a homogeneous landslide mass (input used: ID#12 in Table 2). Key to legend: 1) claystones of the Danisment Formation, 2) slope debris, 3) sliding surfaces, and 4) fault.

Fig. 11 - x-disp values vs. T_l/T_m, T_l^*/T_m and T_s/T_m characteristic period ratios obtained for the Büyükçekmece landslide (solid black line) by considering a heterogeneous landslide composition. AI values range from 0.01 to 1 m/s moving from the left to right columns. Only results referring to 5% (upper row) and 100% (lower row) of the grid nodes are reported here. For AI values of 0.1 m/s, Newmark's displacement and the expected displacement for the earthquake scenario obtained in the MARSite project framework (see Fig. 12 for more details) are also shown.

Fig. 12 - x-disp values vs. T_l/T_m and T_s/T_m characteristic period ratios obtained for the Büyükçekmece landslide (solid black line) by considering a homogeneous landslide composition. AI values range from 0.01 to 1 m/s moving from the left to right columns.

Only results referring to 5% (upper row) and 100% (lower row) of the grid nodes are reported here.

Fig. 13 – Accelerometric signal obtained in the MARSite project framework for the Büyükçekmece landslide area in the case of an earthquake scenario at a 475 yr time period: a) time history, b) Fourier spectrum, c) derived equivalent LEMA_DES signal, and d) properties of the LEMA_DES signal (Lenti and Martino, 2010).

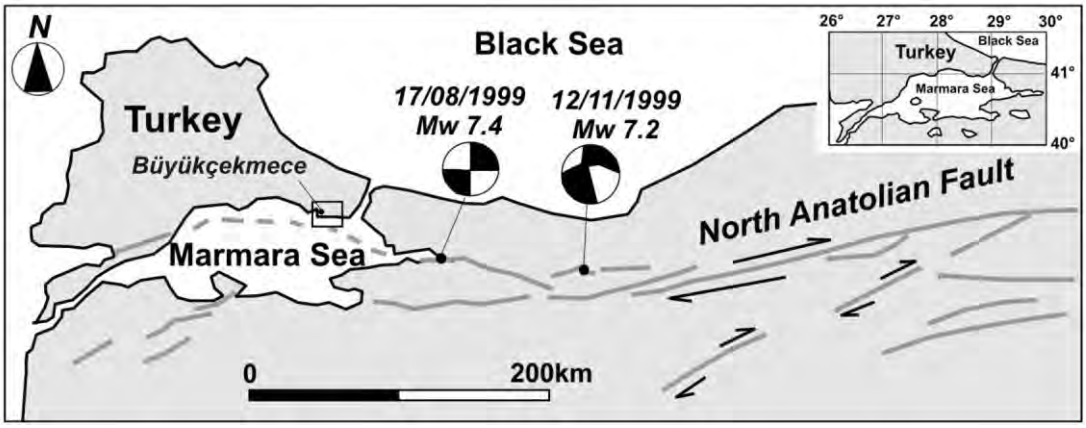

Figure 1

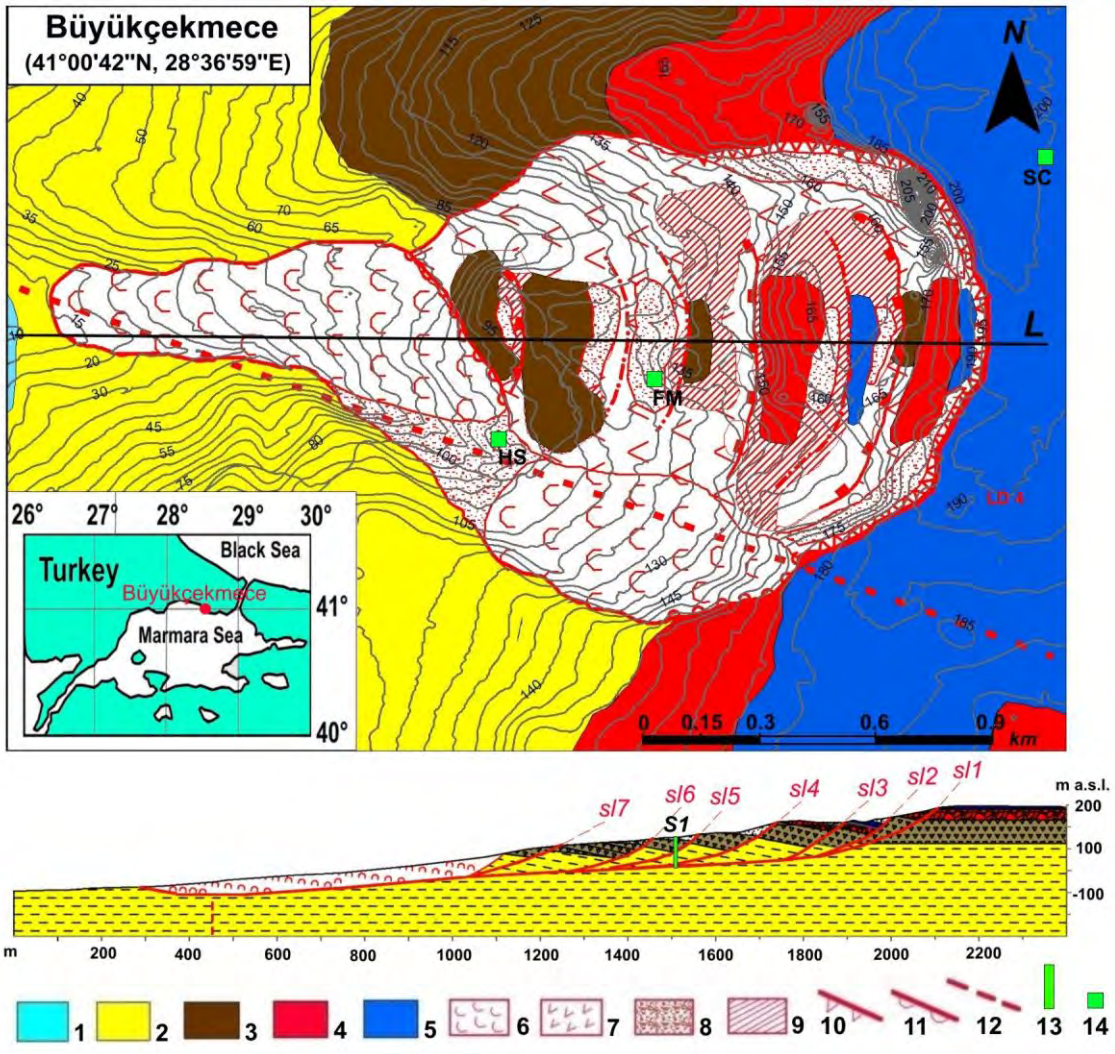

Figure 2

Figure 3

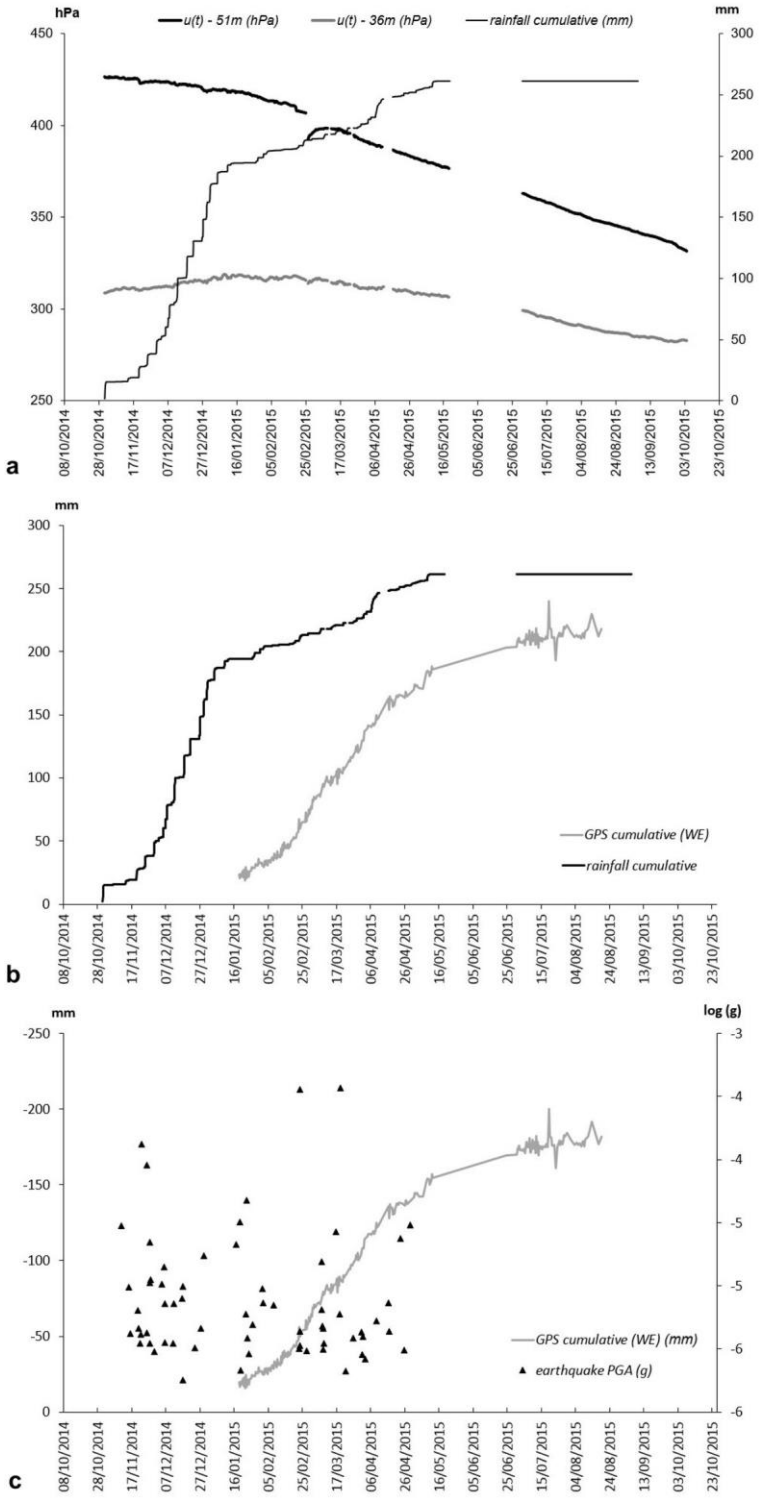

Figure 4

Figure 5

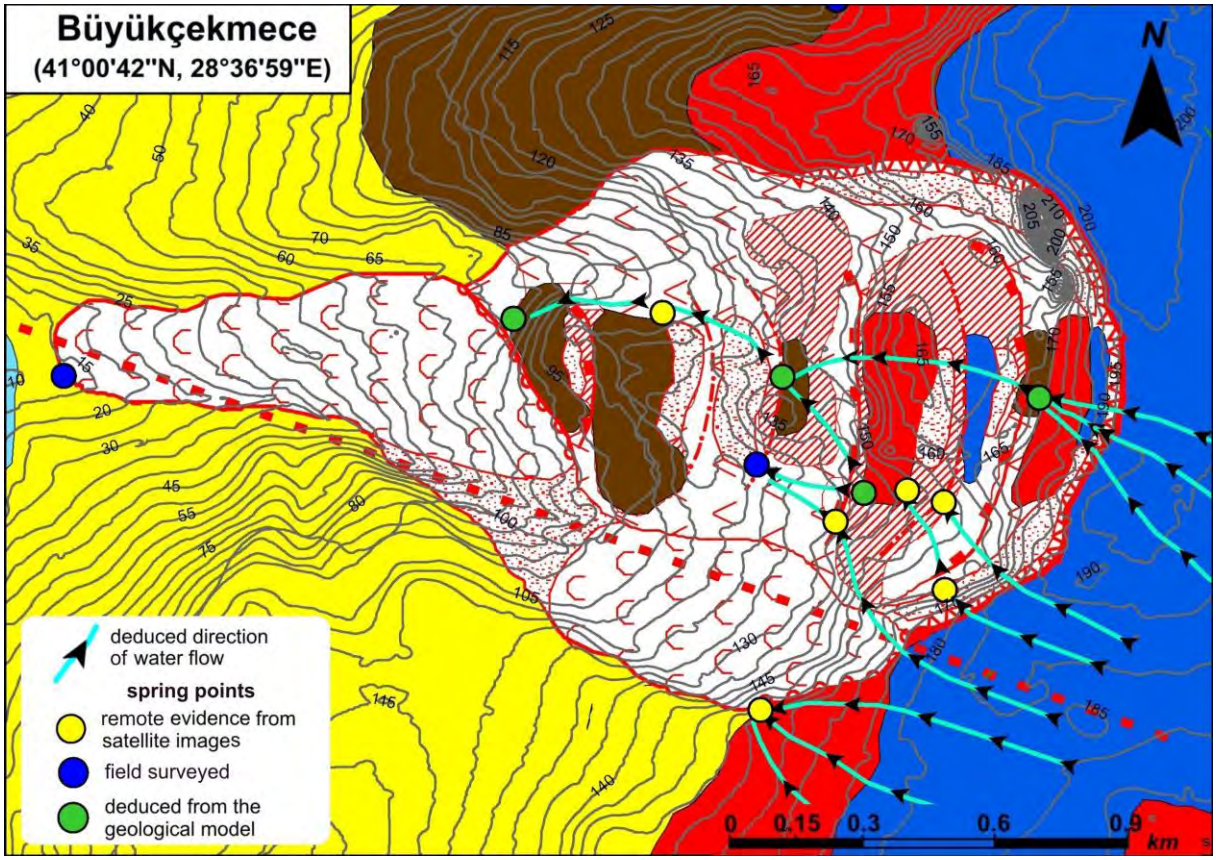

Figure 6

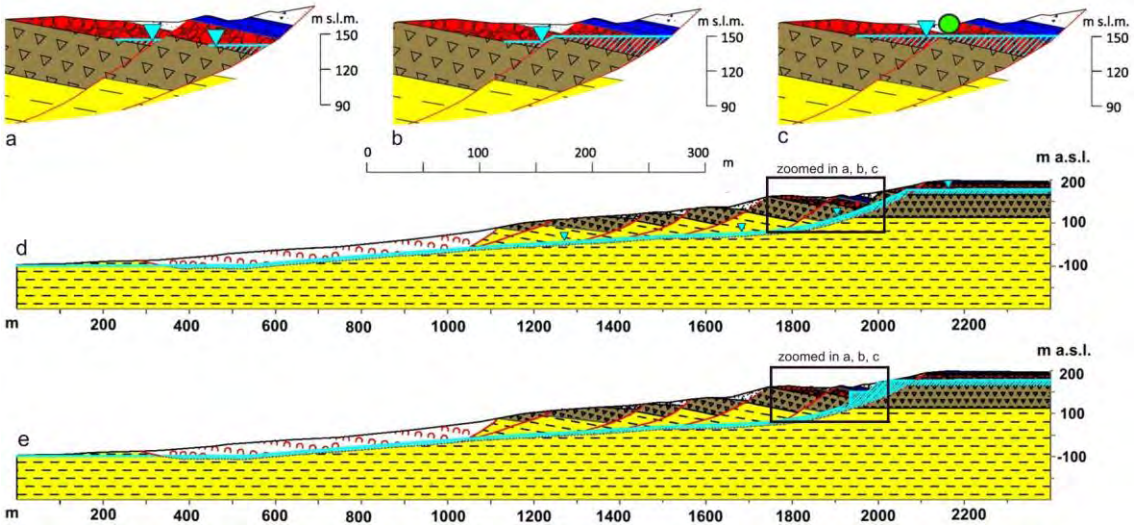

Figure 7

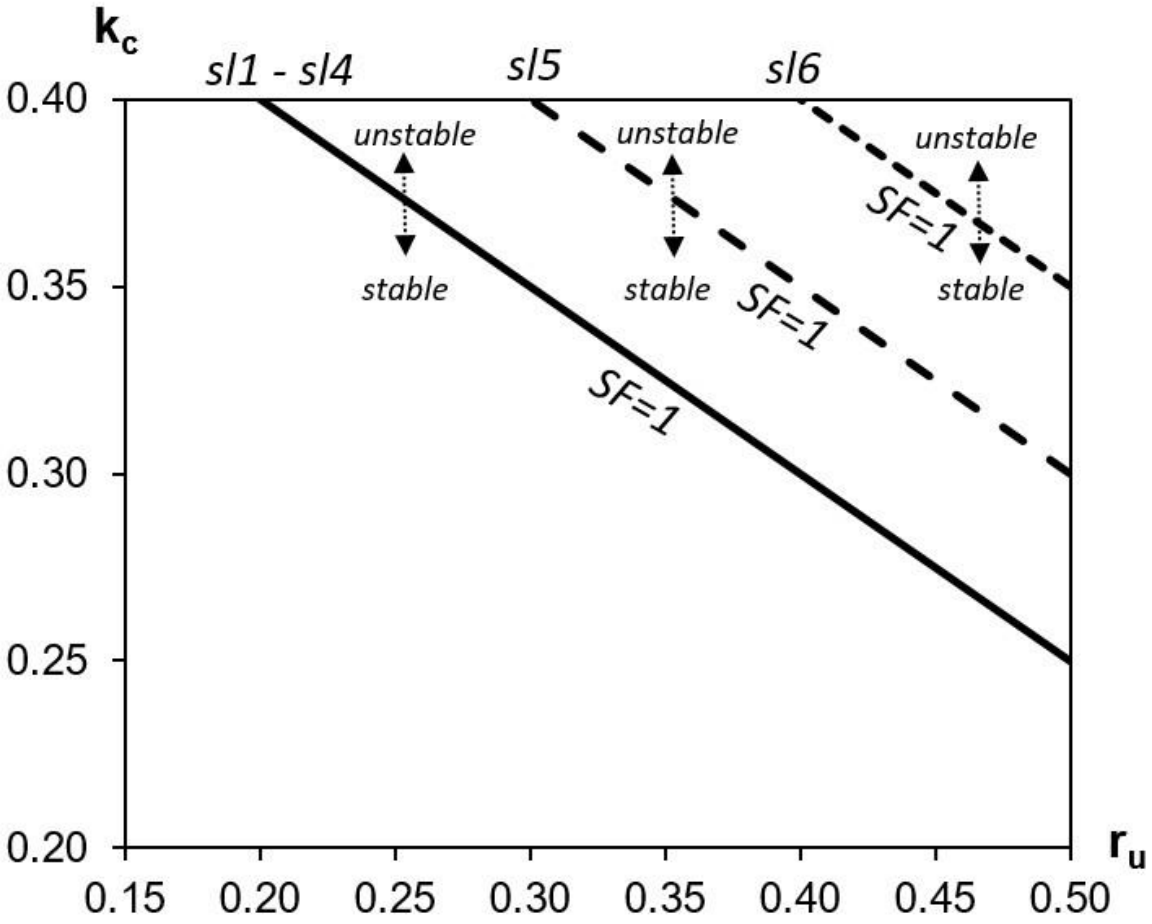

Figure 8

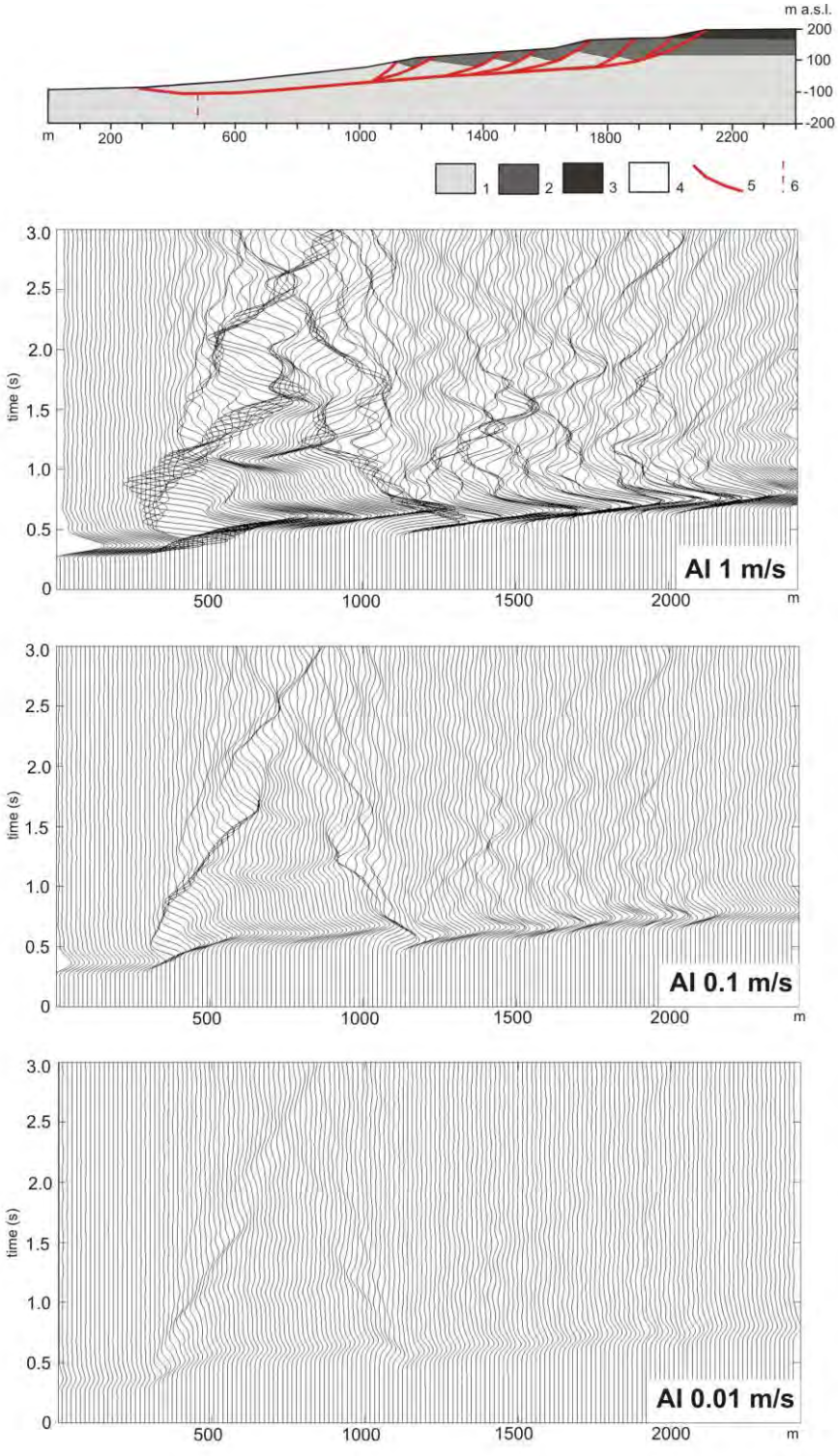

Figure 9

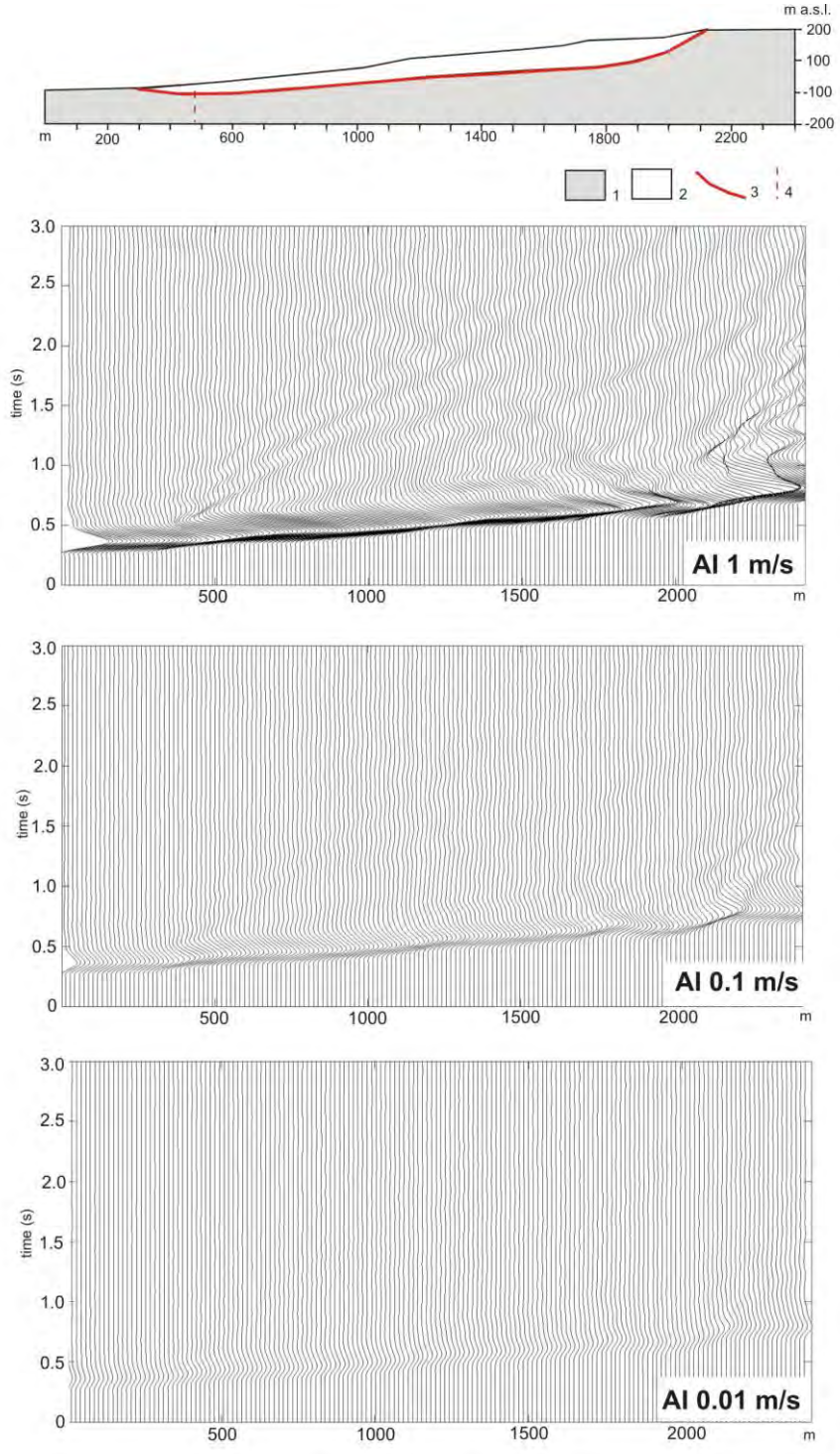

Figure 10

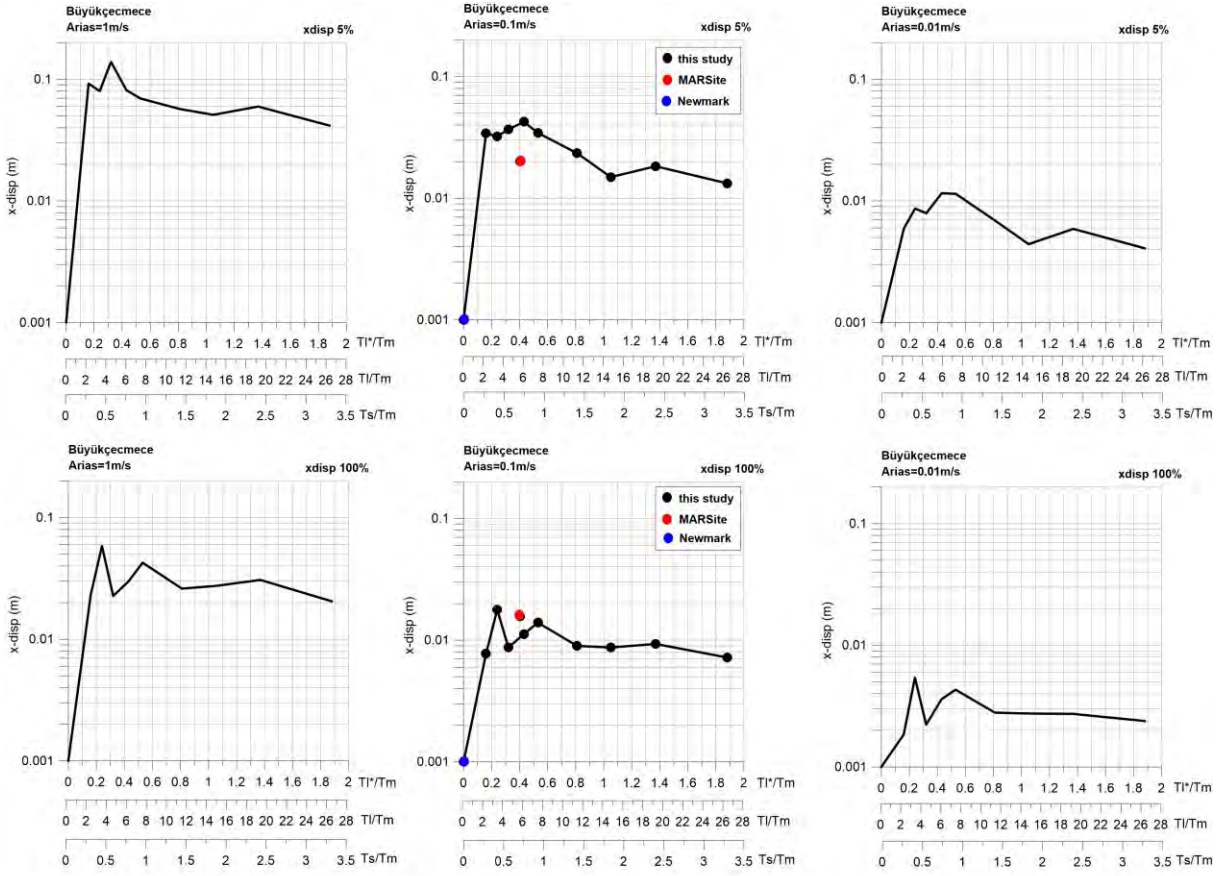

Figure 11

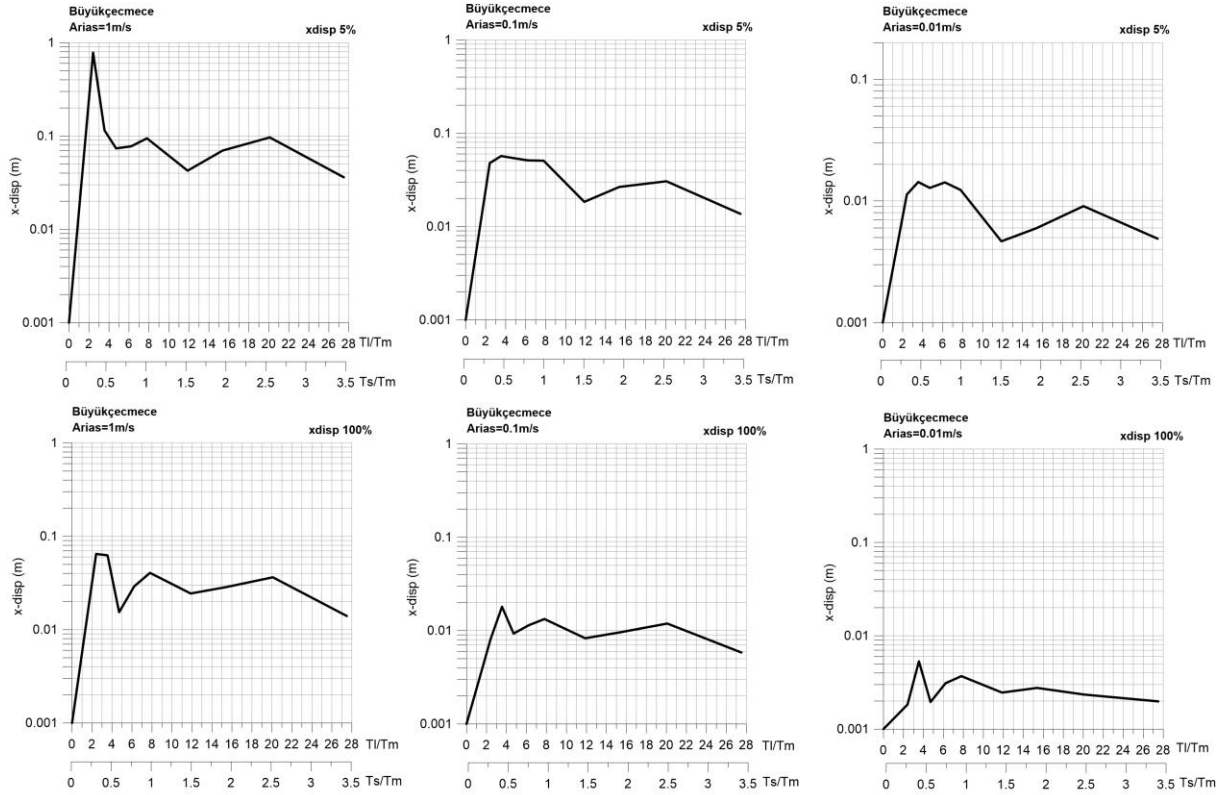

Figure 12

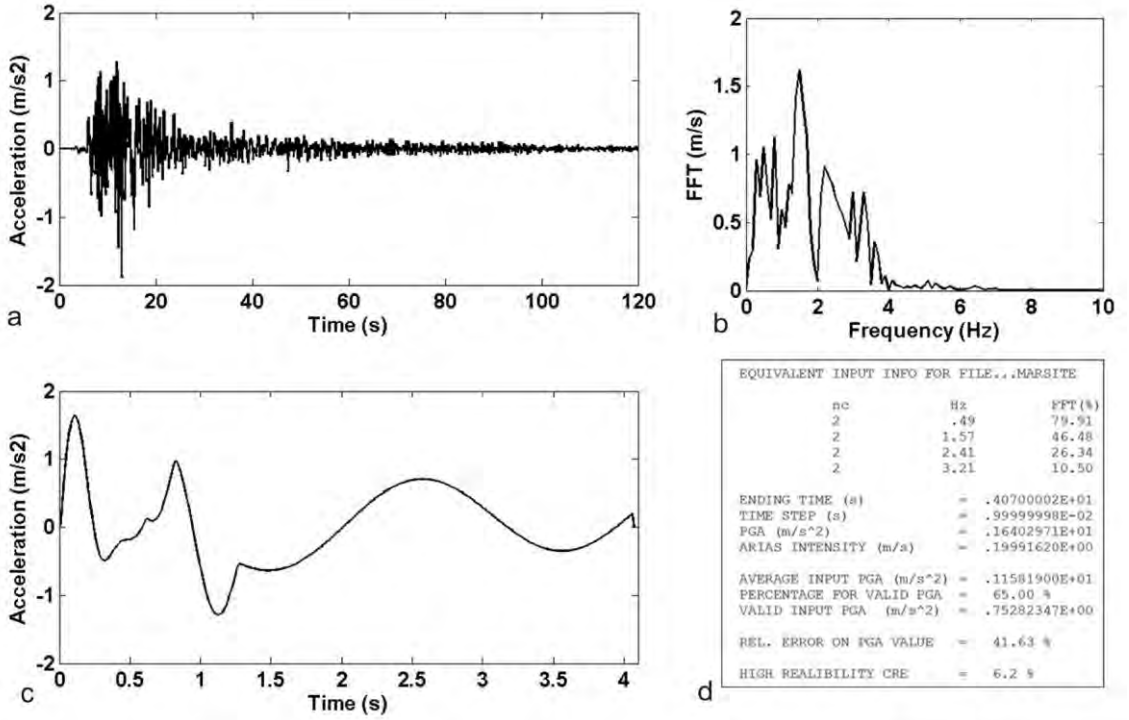

Figure 13

Table 1

litotechnical units	geological formation	Vs (m/s)	Vp (m/s)	density (kg/m^3)	Bulk modulus (MPa)	shear modulus (MPa)	friction angle (°)	cohesion (MPa)	tension (MPa)	dilatancy (°)
Earth-flows debris	Landslide debris	148	259	1800	68.5	39	30	0.2	0.35	5
Debris (dry)		156 - 183	273 – 321	1800	76 - 100	40 - 60	30	0.2	0.35	5
Debris			1079 – 1306		2870 - 3000	41 - 60				
Calcarenites	Bakirköy member of the Çekmece Formation	190 – 255	334 - 445	2400	152 - 270	87 - 154	25	2	2	5
Sands and gravels (dry)	Kiraç member of the Istanbul Formation	203 - 270	357 – 476	1800	105 - 230	87 - 132	35	0.2	0.29	5
Sands and gravels			1600		4490	90				
Clays with tuffs (dry)	Danisment Formation	226 - 373	397 – 656	2000	169 - 274	97 - 157	30	0.2	0.35	5
Clays with tuffs			1571 - 2000		4810 - 7790	97 - 157				
Silty-clays (landslide mass)		366 - 452	642 – 793	2100	491 - 749	281 - 428	24	0.02	0.05	5

Silty-clays (substratum)		600 - 1000	1052 - 1757		1320 - 3680	756 - 2100				10

Table 2

EARTHQUAKES								LEMA_DES signal						Büyükçekmece landslide		
ID#	Location	Date (yyyymmdd)	Epicentral distance (km)	M_w	PGA (m/s^2)	Arias (m/s)	T_m (s)	n_cycles	T_{m_eq} (s)	Duration (s)	Arias_eq (m/s)	PGA_eq (m/s^2)	PGA error (%)	T_s/T_m	T_l/T_m	T_l^*/T_m
1	Tohoku (Japan)	20110311	9700	8.9	4.40E-01	1.88E-01	16.50	/	16.50	41.01	1.88E-01	4.40E-01	/	0.04	0.32	0.02
2	Alpi Apunane (Italy)	20130621	300	5.2	4.00E-01	1.26E-01	7.37	/	7.37	41.15	1.26E-01	4.00E-01	/	0.09	0.71	0.05
3	Serbia	20101103	640	5.4	5.54E-01	1.65E-01	4.02	/	4.02	48.00	1.65E-01	5.54E-01	/	0.16	1.30	0.09
4	Iceland	20000621	11	6.5	4.35E+00	1.15E+00	0.38	2	2.17	9.11	1.20E-01	9.24E-01	62.14	0.29	2.41	0.16
5	Montenegro	19790415	21	7.0	2.11E+00	7.27E-01	0.73	2	1.47	5.65	1.50E-01	1.65E+00	19.17	0.43	3.55	0.24
6	Izmit (Turkey)	19990817	9	7.6	1.58E+00	7.05E-01	0.56	2	1.11	4.57	1.22E-01	1.72E+00	18.71	0.57	4.71	0.32
7	Umbria-Marche (Italy)	19970926	3	5.7	3.37E+00	7.01E-01	0.50	2	0.84	3.43	1.86E-01	1.86E+00	37.78	0.75	6.22	0.43
8	Friuli (Italy)	19760911	9	5.6	2.26E+00	2.74E-01	0.64	3	0.67	3.93	1.55E-01	1.42E+00	18.46	0.94	7.80	0.53
9	Friuli (Italy)	19760511	4	5.0	3.02E+00	3.71E-01	0.30	2	0.44	1.83	1.11E-01	2.11E+00	1.24	1.43	11.87	0.81
10	Friuli (Italy)	19760911	15	5.6	2.31E+00	3.67E-01	0.34	6	0.34	4.13	1.83E-01	1.39E+00	15.73	1.85	15.37	1.05
11	Kozani (Greece)	19950513	17	6.6	2.13E+00	2.65E-01	0.26	1	0.26	0.75	1.20E-01	2.71E+00	95.11	2.42	20.09	1.37
12	Umbria-Marche (Italy)	19980403	10	5.2	3.05E+00	2.45E-01	0.19	2	0.19	0.91	1.13E-01	2.96E+00	88.01	3.31	27.50	1.88